# Comparison Between the Linear and Nonlinear Homogenization of Graphene and Silicon Metasurfaces

QUN REN[1,2], JIAN WEI YOU[1], (Member, IEEE), AND
NICOLAE-CORIOLAN PANOIU[1], (Member, IEEE)
[1]Department of Electronic and Electrical Engineering, University College London, London WC1E 7JE, U.K.
[2]School of Electrical and Information Engineering, Tianjin University, Tianjin 300072, China

Corresponding author: Nicolae-Coriolan Panoiu (n.panoiu@ucl.ac.uk)

**ABSTRACT** In this article, we use a versatile homogenization approach to model the linear and nonlinear optical response of two metasurfaces: a plasmonic metasurface consisting of graphene patches and a dielectric photonic nanostructure consisting of silicon photonic crystal (PhC) cavities. The former metasurface is resonant at wavelengths that are much larger than the graphene elements of the metasurface, whereas the resonance wavelengths of the latter one are comparable to the size of its resonant components. By computing and comparing the effective permittivities and nonlinear susceptibilities of the two metasurfaces, we infer some general principles regarding the conditions under which homogenization methods of metallic and dielectric metasurfaces are valid. In particular, we show that in the case of the graphene metasurface the homogenization method describes very well both its linear and nonlinear optical properties, whereas in the case of the silicon photonic nanostructure the homogenization method is only qualitatively accurate, especially near the optical resonances.

## I. INTRODUCTION

Metamaterials, whose emergence has opened up exciting new opportunities to create novel media with pre-designed physical properties, have been proving to have a significant impact on the development of new approaches and devices for controlling light interaction with matter and achieving key functionalities, including light focusing [1]–[3], perfect lensing [4], [5], perfect absorption [6]–[10], electromagnetic cloaking [11]–[13], imaging with sub-diffraction resolution [14]–[18], and optical sensing [19]–[22]. One of the most important functionalities provided by metamaterials is the enhancement of the local optical field [23]–[30]. This feature is particularly relevant to nonlinear optics since nonlinear optical interactions grow nonlinearly with the applied field. Promising applications of metamaterials can be found in a broad area of science and engineering, including optical

The associate editor coordinating the review of this manuscript and approving it for publication was Derek Abbott.

filters, sensing and infrastructure monitoring, medical devices, remote aerospace applications, and smart solar power management.

As research in metamaterials advanced, it became clear that the two-dimensional (2D) counterpart of metamaterials, the so-called metasurfaces, would offer the fastest route to functional devices and applications. This is so chiefly because most nanofabrication techniques can conveniently be applied to the planar configuration of metasurfaces. These ultrathin and lightweight optical devices are generally made of sub-wavelength dielectric or metallic elements arranged in one-dimensional (1D) or 2D periodic arrays. Equally important from a practical perspective, the single-layer characteristics of photonic devices based on metasurfaces make them particularly amenable to system integration. Because of their small thickness, light-matter interaction occurs in a reduced volume and as such optical losses in metasurfaces are relatively small. Importantly in nonlinear optics applications, this reduced light propagation distance in metasurfaces means that

phase-matching requirements can be relaxed, which greatly reduces the design constraints of nonlinear optical devices based on metasurfaces [31]–[36].

Metasurfaces can mainly be divided into two categories, namely metallic (plasmonic) [37], [38] and dielectric metasurfaces [39], [40]. Plasmonic metasurfaces, which exploit the resonant excitation of surface plasmons at specific frequencies [41]–[43], can greatly enhance the local optical field, but this phenomenon is usually accompanied at optical frequencies by large dissipative losses. Dielectric metasurfaces, on the other hand, experience much smaller optical losses but only provide limited optical field enhancement. Moreover, another difference between the two classes of metasurfaces, which is directly related to the magnitude of the optical losses, is that whereas the resonances in the plasmonic metasurfaces are relatively broad, the resonances associated to dielectric metasurfaces are particularly narrow. As a result, dielectric metasurfaces are usually much more dispersive than the plasmonic ones. One effective approach to study metasurfaces is using homogenization methods [44]–[50], which reduce the metasurface to a homogeneous material with specific retrievable linear and nonlinear optical coefficients. These effective physical quantities are determined in such a way that the metasurface and homogenous layer of material have the same optical response.

In this article, we propose a homogenization method and investigate its accuracy when applied to plasmonic and dielectric metasurfaces. As plasmonic metasurface we consider a graphene metasurface [51]–[54] consisting of a square array of free-standing graphene cruciform patches, whereas the dielectric metasurface is made of a rectangular array of photonic crystal (PhC) cavities possessing high-$Q$ optical modes, embedded in a silicon PhC slab waveguide. The rationale for our choice is that the two metasurfaces capture the general characteristics of the two main classes of metasurfaces, *i.e.* plasmonic and dielectric metasurfaces. In particular, the cruciform graphene patches possess strong plasmon resonances characterized by highly confined, enhanced optical near-field. As optical nonlinearity, we consider second-harmonic generation (SHG) by the nonlocal nonlinear polarization, as symmetry considerations imply that the SHG by the local nonlinear polarization is zero [55], [56]. Moreover, the silicon PhC cavities were designed so as to possess two high-$Q$ optical cavity modes separated by the Raman frequency of silicon, which ensures a strong effective Raman nonlinearity of the silicon photonic nanostructure [57].

The ideas presented in this article are novel in several important aspects. First, we propose a nonlinear homogenization method that does not rely on restrictive, specific assumptions (all that is needed are the relations between the linear fields and nonlinear polarization) and thus is rather general in nature. Second, by choosing two metasurfaces with markedly different but representative physical properties, we investigated and derived several guiding principles regarding the applicability and accuracy of our new nonlinear homogenization method.

The remainder of the paper is organized as follows: In the next section we present the geometrical configurations and material parameters characterizing the two metasurfaces considered in this work. Then, in Sec. III, we introduce the linear and nonlinear homogenization method used to extract the constitutive parameters of the metasurfaces, whereas in Sec. IV we apply our homogenization approach to the two metasurfaces and derive general principles regarding the conditions in which the predictions of the homogenization method are valid. In particular, we extract the linear and nonlinear constitutive parameters of the metasurfaces and then compare the optical response of the metasurfaces with that of their homogenized counterparts. Finally, we conclude our paper by summarizing the main findings of our study and discussing some of their implications to future developments pertaining to metamaterials research.
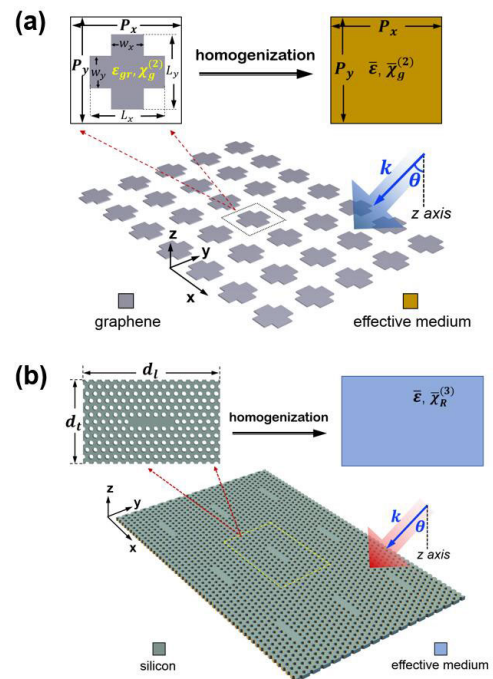


**FIGURE 1.** Schematic of homogenization of two metasurfaces. (a) Geometry of a graphene metasurface consisting of a 2D array of graphene crosses. The unit cell is homogenized into a uniform layer of material characterized by effective parameters. (b) Geometry of a silicon photonic nanostructure consisting of a rectangular array of silicon PhC nanocavities in a hexagonal PhC slab waveguide made of silicon. The unit cell is homogenized into a uniform layer of material with effective parameters.

## II. DESCRIPTION OF THE GRAPHENE AND SILICON METASURFACES

In this section, we describe the geometrical configuration and material parameters of the two metasurfaces investigated in this work, namely the graphene cruciform metasurface illustrated in figure 1(a) and the silicon photonic nanostructure shown in figure 1(b). In addition, we explain the rationale for our choice of metasurfaces by presenting their main physical properties.

## A. GEOMETRICAL CONFIGURATION OF THE GRAPHENE AND SILICON METASURFACES

The graphene metasurface lies in the $x$-$y$ plane and consists of a square array of cruciform graphene patches. The symmetry axes of the array coincide with the $x$- and $y$-axes and are oriented along the arms of the crosses, as per figure 1(a). The length and width of the arms of the crosses along the two axes are $L_x$ ($L_y$) and $w_x$ ($w_y$), respectively, whereas the corresponding periods of the metasurface are $P_x$ and $P_y$. In this, work, unless otherwise specified, $L_x = L_y = 60$ nm, $w_x = w_y = 30$ nm, and $P_x = P_y = 100$ nm, meaning that the crosses are symmetric. Graphene metasurfaces with similar geometrical parameters have been recently investigated both experimentally and theoretically (for a review of fabrication and theory of optical structures made of graphene and other 2D materials see Ref. [58]).
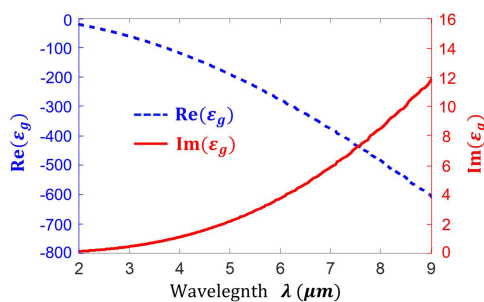
The relative electric permittivity of graphene is given by the relation:

$$\varepsilon_g = 1 + \frac{i\sigma_s}{\varepsilon_0 \omega h_g}, \qquad (1)$$

where $h_g = 0.3$ nm is the thickness of graphene, $\omega$ is the frequency, and the graphene surface conductivity, $\sigma_s$, is described by the Kubo's formula [59]:

$$\sigma_s = \frac{e^2 k_B T \tau}{\pi \hbar^2 (1 - i\omega\tau)} \left[ \frac{\mu_c}{k_B T} + 2 \ln \left( e^{-\frac{\mu_c}{k_B T}} + 1 \right) \right] + \frac{ie^2}{4\pi\hbar} \ln \frac{2|\mu_c|\tau/\hbar - i(1 - i\omega\tau)}{2|\mu_c|\tau/\hbar + i(1 - i\omega\tau)}. \qquad (2)$$

Here, $\mu_c$, $T$, and $\tau$ are the chemical potential, temperature, and relaxation time, respectively. In this study, unless otherwise specified, we use $\mu_c = 0.6$ eV, $\tau = 0.1$ ps, and $T = 300$ K.

**FIGURE 2.** Wavelength dependence of the real and imaginary parts of the graphene relative permittivity.

The wavelength dependence of the real and imaginary parts of graphene permittivity, as described by Eq. (1) in conjunction with Eq. (2), are depicted in figure 2. It can be seen in this figure that $\Im\mathfrak{m}(\varepsilon_g) > 0$ and $\Re\mathfrak{e}(\varepsilon_g) < 0$, which are characteristics shared by most noble metals.

The silicon photonic nanostructure, illustrated in figure 1(b), consists of a rectangular array of PhC cavities embedded in a PhC slab waveguide made of silicon ($n_{Si} = 3.4$) [57]. The PhC slab waveguide comprises a 2D
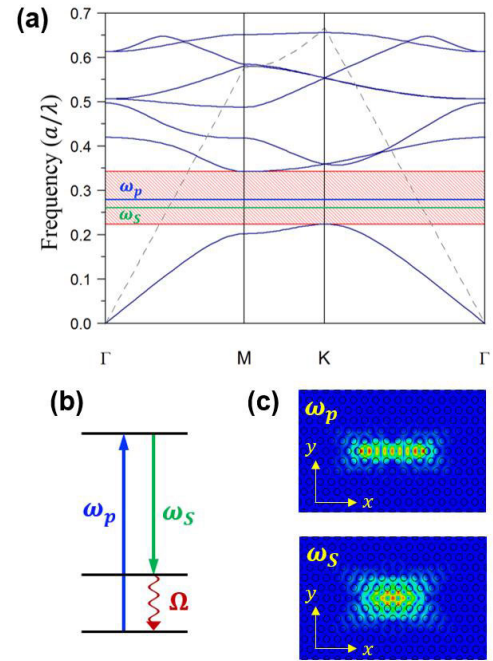
**FIGURE 3. a)** Transverse-magnetic band structure of the PhC and two optical modes of the PhC cavity withe frequencies of $\omega_p$ and $\omega_S$. The dashed lines indicate light lines. b) Diagrammatic representation of the stimulated Raman scattering. c) The field profiles of the optical modes at the pump and Stokes frequencies.

hexagonal lattice of air holes in a silicon slab with the hole radius $r = 0.29a$ and slab thickness $t = 0.6a$, where $a$ is the lattice constant. Moreover, the optical nanocavities are the so-called $L5$ PhC cavities, namely they are created by filling in 5 consecutive holes oriented along the $\Gamma K$ symmetry axis of the hexagonal lattice. The periods of the PhC metasurface, defined as the center-to-center distance along the $x$- and $y$-axes between adjacent PhC cavities, are $d_l = 17a$ and $d_t = 6\sqrt{3}a$, respectively. In order to increase the $Q$-factor of the optical modes of this PhC nanocavity, we shifted outwardly the end-holes of the cavity by $0.15a$ [60].

The PhC cavity is designed in such a way that it possesses two optical modes whose frequencies are separated by the Raman frequency of silicon, $\Omega = 2\pi \times 15.6$ THz [61]. This ensures a very strong nonlinear coupling between the two optical modes, both because of the large optical field enhancement inside the cavities and also due to favorable spatial overlap between the two optical modes. Consequently, one can achieve an efficient Raman interaction between the two optical modes. This means that the PhC nanocavities can be viewed as artificially engineered, strongly nonlinear "silicon meta-atoms", which when arranged in some spatial pattern give rise to photonic metasurfaces with large Raman nonlinearity. In particular, if one chooses the lattice constant $a = 333$ nm, the resonance frequency of the pump and Stokes modes are $\omega_p = 1572.5$ THz and $\omega_S = 1474.6$ THz, respectively, and therefore the condition $\omega_p - \omega_S = \Omega$ is fulfilled. Expressed in terms of normalized frequency of $2\pi c/a$, the frequencies of the two optical modes are

$\omega_p = 0.2778$ and $\omega_S = 0.2605$. Also, the $Q$-factors of the two modes are $Q_p = 1804$ and $Q_S = 1.12 \times 10^5$.
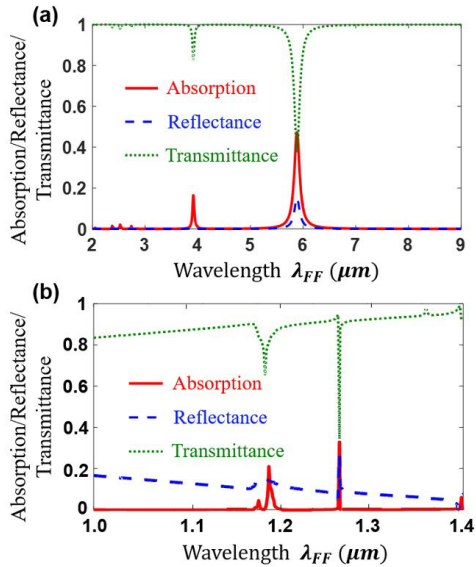


**FIGURE 4.** a) Wavelength dependence of absorption, reflectance, and transmittance of the graphene metasurface. b) The same as in a), but determined for the silicon photonic nanostructure.

The linear optical response of graphene and silicon metasurfaces are presented in figures 4(a) and 4(b), respectively. In all cases considered in this work, unless otherwise specified, the incident wave was an *x*-polarized plane wave normally incident onto the metasurface (an experimental set-up for the measurement of transmittance, reflectance, and absorption at normal or near-normal incidence can be found in [62]). Due to the symmetry properties of the unit cell, the optical response of the graphene metasurface does not depend on the polarization of the incident wave, but such a dependence does exist in the case of the silicon metasurface. Figure 4 clearly shows that, in the case of the graphene metasurface, absorption, *A*, reflectance, *R*, and transmittance, *T*, have a series of spectral resonances occurring at common wavelengths. These resonances are due to the generation of localized surface plasmons in the graphene crosses, the resonance wavelength of the fundamental plasmon being $\lambda = 5.88 \, \mu\text{m}$. It can also be seen that the excitation of surface plasmons is accompanied by a large increase of the optical absorption, which suggests that at the corresponding resonance wavelengths the optical near-field is significantly enhanced. Moreover, the spectra of the silicon photonic nanostructure show two resonances at the frequencies of the two cavity modes, the width of these resonances being much smaller than that of plasmon resonances.

### B. MOTIVATION FOR CHOICE OF UNIT CELLS
Our choice for the unit cells of the two metasurfaces was guided by the following two ideas: First, the unit cells should contain resonant elements that generate strong enhancement of the optical near-field. This, in turn, would ensure a large

enhancement of the nonlinear optical response of the metasurfaces. Second, the elements of the unit cells should be generic enough, namely the structure of the elements in the unit cells should not be too simple, which would restrict the validity of our findings, but at the same time they should not have a very complicated structure, which would perhaps limit the generality of the conclusions of our study.

The two metasurfaces investigated in this article satisfy these two criteria. Thus, the graphene crosses and our specially engineered PhC cavity support localized surface plasmons and a set of optical modes separated by silicon Raman frequency, respectively, so that in both cases strong enhancement of the optical nonlinearity can be achieved. Moreover, the structure of the graphene patches is complex enough to allow one to study additional phenomena, such as polarization-dependent optical response, by simply altering its geometrical parameters. In particular, we wanted to avoid using simple geometries, such as circular or square graphene patches, as one might have been led to believe that the conclusions of our work would be limited to these simple cases. Furthermore, in order to increase the generality of our work, we chose to use neither highly engineered PhC cavities, nor simple designs of PhC cavities, which usually possess optical modes with low $Q$-factors.

### III. LINEAR AND NONLINEAR HOMOGENIZATION METHOD
In this section, we present first the homogenization approach used to describe the effective optical response of the metasurfaces investigated in this article and retrieve their effective permittivities and nonlinear susceptibilities and then compare the linear optical response of the original and homogenized metasurfaces so as to clarify the circumstances in which our homogenization approach is accurate.

### A. THEORY OF THE EFFECTIVE PERMITTIVITY OF METASURFACES
The general linear homogenization method presented here amounts to establishing a relationship between the averaged electric displacement field, *D*, and the electric field, *E*, and is known as the field averaging method. It will be expanded later on to the nonlinear case. As it is well known, the constitutive relation of a linear anisotropic material is expressed as $D_i = \sum_j \epsilon_{ij} E_j$, where $\epsilon_{ij}$ is the permittivity tensor and the subscripts $i, j = x, y, z$. The field-average method relies on this relation, the effective permittivity of the medium being defined via a similar relation between the electric field and the electric displacement field:

$$\overline{\mathbf{E}}(\omega) = \frac{1}{V} \int_V \mathbf{E}(\mathbf{r}, \omega) d\mathbf{r}, \tag{3}$$

$$\overline{\mathbf{D}}(\omega) = \frac{1}{V} \int_V \mathbf{D}(\mathbf{r}, \omega) d\mathbf{r}. \tag{4}$$

This method is particularly suitable for describing metasurfaces, because in this case the averaging domain can be naturally defined as the unit cell of the metasurface. Therefore,

in the equations above, $V$ is the volume of the unit cell of the metasurface.

According to the field averaging method, for an isotropic medium whose permittivity tensor is diagonal, the effective permittivity is evaluated as $\overline{\epsilon}_i = \overline{D}_i/\overline{E}_i$. This definition can be extended to anisotropic media as follows: First, one defines an auxiliary quantity, $d_{ij} = \epsilon_{ij}E_j$, and express the displacement field as $D_i = \sum_j d_{ij}$, and then calculate the averaged value of each component of the auxiliary quantity:

$$\overline{d}_{ij}(\omega) = \frac{1}{V}\int_V d_{ij}(\mathbf{r}, \omega)d\mathbf{r} = \frac{1}{V}\int_V \epsilon_{ij}(\mathbf{r}, \omega)E_j(\mathbf{r}, \omega)d\mathbf{r}. \quad (5)$$

If we assume that the averaged fields are related by a constitutive relation similar to that corresponding the local fields, namely $\overline{D}_i = \sum_j \overline{\epsilon}_{ij}\overline{E}_j$, and by requiring that the average of the field $\mathbf{D}(\mathbf{r}, \omega)$ of the metasurface and the field $\overline{\mathbf{D}}(\omega)$ in the homogenized layer of material are termwise equal, the effective permittivity is determined by the following equation:

$$\overline{\epsilon}_{ij}(\omega) = \frac{\overline{d}_{ij}(\omega)}{\overline{E}_j(\omega)} = \frac{\int_V \epsilon_{ij}(\mathbf{r}, \omega)E_j(\mathbf{r}, \omega)d\mathbf{r}}{\int_V E_j(\mathbf{r}, \omega)d\mathbf{r}}. \quad (6)$$

This formula has been used to determine the effective permittivity of both metasurfaces. Before moving on to the calculation of the effective nonlinear susceptibilities of the metasurfaces, we note that in the case of the graphene metasurface the volume integrals can be reduced to surface integrals across the midsection of the graphene sheet because the fields across the ultrathin graphene layer vary only slightly.

## B. CALCULATION OF EFFECTIVE SECOND-ORDER SUSCEPTIBILITY OF GRAPHENE METASURFACES

As we assume that the graphene crosses are free standing, symmetry considerations imply that the dipole (local) nonlinear polarization at the second harmonic (SH) exactly cancels. Consequently, the lowest order SHG is due to the nonlocal nonlinear polarization whose sources are magnetic dipoles and electric quadrupoles oscillating at the SH frequency. It should be noted that if the graphene patches lie onto a substrate the inversion symmetry is broken and consequently the generated SH is due to the dipole nonlinear polarization. The homogenization of such graphene metasurfaces has been recently studied [63].

This nonlinear polarization and the associated nonlinear surface current in the case of graphene metasurfaces characterized by nonlocal nonlinear polarization can be expressed as [55]:

$$\mathbf{P}(\mathbf{r}, \Omega) = \epsilon_0\boldsymbol{\chi}_g^{(2)}(\Omega; \omega, \omega)\vdots\mathbf{E}(\mathbf{r}, \omega)\nabla\mathbf{E}(\mathbf{r}, \omega), \quad (7)$$

$$\mathbf{J}_s(\mathbf{r}, \Omega) = \boldsymbol{\sigma}_g^{(2)}(\Omega; \omega, \omega)\vdots\mathbf{E}(\mathbf{r}, \omega)\nabla\mathbf{E}(\mathbf{r}, \omega), \quad (8)$$

where $\boldsymbol{\chi}_g^{(2)}(\Omega; \omega, \omega)$ and $\boldsymbol{\sigma}_g^{(2)}(\Omega; \omega, \omega)$ are the *bulk* nonlinear second-order susceptibility and *surface* nonlinear second-order optical conductivity, respectively, and are related by the

following formula:

$$\boldsymbol{\chi}_g^{(2)}(\Omega; \omega) = \frac{i}{\epsilon_0\Omega h_g}\boldsymbol{\sigma}_g^{(2)}(\Omega; \omega). \quad (9)$$

We note that instead of a bulk nonlinear susceptibility one can use a surface one, defined as $\boldsymbol{\chi}_{s,g}^{(2)} = h_g\boldsymbol{\chi}_g^{(2)} = (i/\epsilon_0\Omega)\boldsymbol{\sigma}_g^{(2)}$, but we decided to use bulk quantities so that it is more convenient to compare these nonlinear optical coefficients of graphene with those of other centrosymmetric materials.

The surface nonlinear second-order optical susceptibility of graphene has been recently derived in [64] and is given by the following equation:

$$\sigma_{g,ijkl}^{(2)}(\Omega; \omega) = \sigma_{g,\Omega}^{(2)}(\omega)\left(\delta_{ik}\delta_{jl} - \frac{5}{3}\delta_{ij}\delta_{kl} - \frac{1}{3}\delta_{il}\delta_{jk}\right), \quad (10)$$

where the scalar part of the surface second-order conductivity tensor is:

$$\sigma_{g,\Omega}^{(2)}(\omega) = \frac{3e^3\mu_c^2\tau^3}{8\pi\hbar^2(1 - i\omega\tau)^3}. \quad (11)$$

Componentwise, the nonlinear polarization can be evaluated as:

$$P_i(\mathbf{r}, \Omega) = \epsilon_0\sum_{jkl}\chi_{g,ijkl}^{(2)}E_j(\mathbf{r}, \omega)\nabla_k E_l(\mathbf{r}, \omega) \equiv \sum_{jkl}q_{ijkl} \quad (12)$$

where we introduced a new nonlinear auxiliary quantity defined as $q_{ijkl} = \epsilon_0\chi_{g,ijkl}^{(2)}E_j\nabla_k E_l$. Moreover, the spatial average of this quantity is:

$$\overline{q}_{ijkl}(\Omega) = \frac{1}{V}\int_V \epsilon_0\chi_{ijkl}^{(2)}(\mathbf{r})E_j(\mathbf{r}, \omega)\nabla_k E_l(\mathbf{r}, \omega)d\mathbf{r}, \quad (13)$$

where $\chi_{ijkl}^{(2)}(r) = \chi_{g,ijkl}^{(2)}$ if $r$ corresponds to a point inside the graphene crosses and $\chi_{ijkl}^{(2)}(\mathbf{r}) = 0$ if $\mathbf{r}$ is in the air region.

If we express the nonlinear polarization in the homogenized metasurface as:

$$\overline{P}_i(\Omega) = \epsilon_0\sum_{jkl}\overline{\chi}_{ijkl}^{(2)}\overline{E}_j(\omega)\overline{\nabla_k E_l}(\omega), \quad (14)$$

where $\overline{\chi}_{ijkl}^{(2)}$ is the effective nonlinear second-order susceptibility of the homogenized metasurface, and impose the condition that the spatial average of the nonlinear polarization described by Eq. (12) is *termwise* equal to the polarization in Eq. (14), we obtain the following formula for the effective nonlinear susceptibility:

$$\overline{\chi}_{ijkl}^{(2)}(\Omega; \omega) = \frac{\overline{q}_{ijkl}}{\overline{E}_j\overline{\nabla_k E_l}}. \quad (15)$$

In this formula and in Eq. (14), the quantity $\overline{\nabla_i E_j}$ is defined as:

$$\overline{\nabla_i E_j} = \frac{1}{V}\int_V \nabla_i E_j(\mathbf{r}, \omega)d\mathbf{r}. \quad (16)$$

## C. THEORY OF EFFECTIVE RAMAN SUSCEPTIBILITY OF SILICON PHOTONIC NANOSTRUCTURES

The calculation of the effective Ramman susceptibility of the silicon based photonic nanostructure described in Sec. 2 is similar to that of the effective second-order susceptibility presented in the preceding subsection, so that here we present only the main steps. A more detailed derivation can be found in [57].

We start our analysis with the nonlinear Raman polarization at the Stokes frequency, $\mathbf{P}_R(\mathbf{r}, \omega_S)$, which can be written as:

$$\mathbf{P}_R(\mathbf{r}, \omega_S) = \frac{3}{2}\epsilon_0 \chi_R^{(3)}(\mathbf{r}) \vdots \mathbf{E}(\mathbf{r}, \omega_p)\mathbf{E}^*(\mathbf{r}, \omega_p)\mathbf{E}(\mathbf{r}, \omega_S), \quad (17)$$

where $\chi_R^{(3)}(\mathbf{r})$ is the Raman susceptibility and $\mathbf{E}(\mathbf{r}, \omega_p)$ and $\mathbf{E}(\mathbf{r}, \omega_S)$ are the optical fields at the pump and Stokes frequencies, respectively. For the sake of simplicity, we assume that the symmetry axes of the array of PhC cavities coincide both with the $x$- and $y$-axes and with the principal axes of silicon. Under these circumstances, the nonzero components of $\chi_R^{(3)}$ are $\chi_{R,ijij}^{(3)} = \chi_{R,jiji}^{(3)} = \chi_{R,jiij}^{(3)} = \chi_{R,ijji}^{(3)}$, with $i, j = x, y, z$ and $i \neq j$. The value at resonance of the only independent component is $\chi_{R,1212}^{(3)} = -i11.2 \times 10^{-18} \, \text{m}^2 \, \text{V}^{-2}$ [65].

We then define the spatially averaged effective Raman polarization:

$$\overline{\mathbf{P}}_R(\omega_S) = \frac{1}{V}\int_V \mathbf{P}_R(\mathbf{r}, \omega_S)d\mathbf{r}, \quad (18)$$

where the volume integration is taken over the unit cell of the metasurface, together with the effective Raman polarization in a homogenized slab of nonlinear optical medium with the same thickness as that of the PhC slab:

$$\mathbf{P}_R^{\text{eff}}(\omega_S) = \frac{3}{2}\epsilon_0 \overline{\chi}_R^{(3)} \vdots \overline{\mathbf{E}}(\omega_p)\overline{\mathbf{E}}^*(\omega_p)\overline{\mathbf{E}}(\omega_S). \quad (19)$$

Here, $\overline{\chi}_R^{(3)}$ is the effective Raman susceptibility of the homogenized metasurface.

As in the case of the graphene metasurface, we cannot simply impose the condition that the components of the nonlinear polarizations in Eq. (18) and Eq. (19) are equal because in the general case the effective Raman susceptibility tensor, $\overline{\chi}_R^{(3)}$, has 81 independent components, so that the corresponding system of equations is overdetermined. Consequently, we impose the condition that the r.h.s. of equations Eq. (18) and Eq. (19) are *termwise identical*. Using this constraint, it can be seen that the components of $\overline{\chi}_R^{(3)}$ are determined by the following formula:

$$\overline{\chi}_{R,ijkl}^{(3)} = \frac{\frac{1}{V}\int_V \chi_{R,ijkl}^{(3)}(\mathbf{r})E_j(\mathbf{r}, \omega_p)E_k^*(\mathbf{r}, \omega_p)E_l(\mathbf{r}, \omega_S)d\mathbf{r}}{\overline{E}_j(\omega_p)\overline{E}_k^*(\omega_p)\overline{E}_l(\omega_S)}. \quad (20)$$

Note that the components of $\overline{\chi}_R^{(3)}$ and $\chi_R^{(3)}$ cancel for the same set of indices $i, j, k,$ and $l$.

Before we move on to the description of our computational approach, we want to make it clear that our homogenization

method does not simply rely on the quasistatic approximation because the linear fields are calculated rigorously. This means that retardation and multiple scattering effects present in the photonic crystal regime are rigorously taken into account. The main approximation we make is that the nonlocal effects on the effective permittivity of the structure are neglected, which is equivalent to neglecting the dependence of the effective permittivity and effective nonlinear susceptibility on the wave vector, $\mathbf{k}$. In other words, we determine $\overline{\epsilon}(\omega, \mathbf{k})|_{\mathbf{k}=0}$ and $\overline{\chi}(\omega, \mathbf{k})|_{\mathbf{k}=0}$.
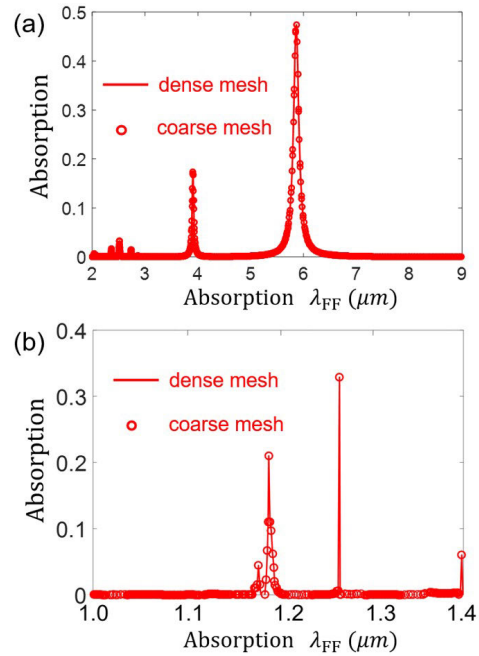
**FIGURE 5. a)** Absorption spectra of the graphene metasurface calculated using a computational mesh with at least 20 cells per wavelength (solid lines) and at least 10 cells per wavelength (circles). **b)** The same as in a), but determined for the silicon photonic nanostructure.

## D. COMPUTATIONAL APPROACH

In our calculation of the transmittance, reflectance, and absorption spectra of the graphene and silicon photonic nanostructures we used a finite-element frequency-domain solver, as implemented in the commercial software CST STUDIO [66]. Along the $x$- and $y$-axes we used periodic boundary conditions, whereas along the $z$-axis we used open-add-space boundary conditions. Moreover, in all our calculations we used 20 cells per wavelength. However, we observed that in most cases converged results can be obtained as long as there are at least 10 cells per wavelength. In order to illustrate this finding, we present in figure 5 the absorption spectra of the graphene and silicon metasurfaces, corresponding to two computational meshes, namely a coarse mesh containing at least 10 cells per unit length and a finer one containing at least 20 cells per wavelength. For the nonlinear simulation, we used a hybrid numerical method, combing the finite-difference time-domain (FDTD) method and the nonlinear

generalized source (GS) method, as detailed in our previous work [67].

The photonic band structure of the PhC slab and the corresponding cavity modes were computed with RSoft's BandSOLVE [68], with the cavity modes lying in the transverse-magnetic bandgap of the PhC slab waveguide (see figure 3). In order to calculate the cavity modes, we used a supercell with size $7a \times 7a \times 4a$ and $224 \times 224 \times 128$ plane-waves, that is, 32 plane-waves per lattice constant, $a$. Moreover, the $Q$-factors of the optical cavity modes have been calculated using the finite-difference time-domain method as implemented in MEEP [69], a freely available software.

In our numerical simulations we used a workstation with a 10-core Intel® Xeon® processor E5-2660 v3 @ 2.60 GHz and 25 MB cache memory. Generic simulation times for the silicon photonic nanostructure and its homogenized counterpart were 270 min and 10 min, respectively, whereas in the case of the graphene metasurface generic simulation times for the metasurface and its homogenized counterpart were 120 min and 15 min, respectively. These results show a reduction of about an order of magnitude of the computational time in the case of the homogenized structure as compared to that corresponding to the actual metasurface.

## IV. RESULTS AND DISCUSSIONS

In this section, we study the circumstances in which our method produces accurate results and use it to understand the main differences between the physical properties of graphene and silicon PhC metasurfaces.

### A. EFFECTIVE PERMITTIVITIES OF THE GRAPHENE AND SILICON PHOTONIC CRYSTAL METASURFACES

Based on our theoretical analysis, the effective permittivity of the two metasurfaces investigated in this work can be calculated using Eq. (6). The results of our calculations, corresponding to the graphene and silicon PhC metasurfaces, are presented in figure 6(a) and figure 6(b), respectively. These figures show some similarities between the two spectra but also significant differences. Thus, the effective permittivity of graphene metasurface displays a series of spectral resonances of Lorentzian nature, which occur at the plasmon resonance wavelengths of the graphene crosses. This means that the graphene crosses behave as meta-atoms that possess a series of resonant states, the overall optical response of the metasurface being primarily determined by these resonances. The main reason for this behavior can be traced to the size of the graphene crosses relative to the resonance wavelengths of the plasmons of the graphene crosses. Specifically, since the size of the crosses is much smaller than the plasmon wavelengths, the overall optical response of the graphene metasurface can be viewed as a superposition of the response of weakly interacting Lorentz-type oscillators. It should be noted that since the resonance wavelength of graphene plasmons is usually much larger than the size of graphene patches, one could not have a situation in which the conditions that the operating wavelength is comparable to the size of graphene

patches and the optical near-field is strongly enhanced *via* plasmon excitation are simultaneously satisfied.
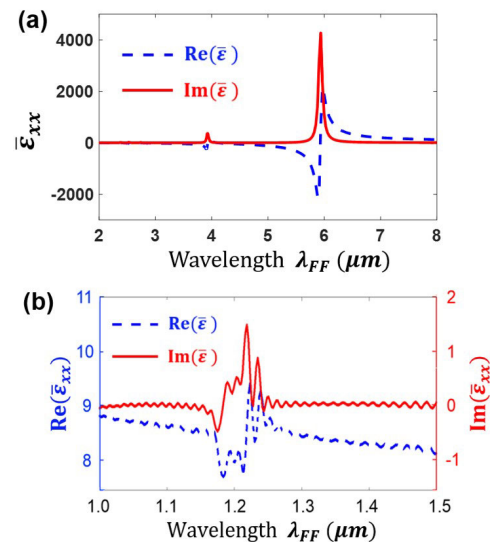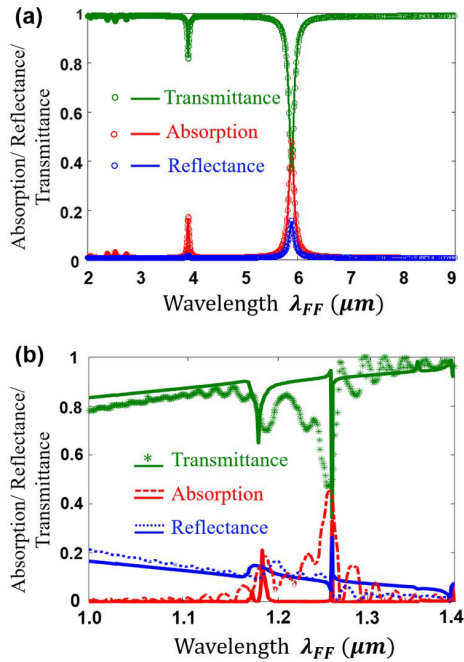


**FIGURE 6.** a) Spectra of the real and imaginary parts of the effective permittivity of the graphene metasurface. b) The same as in a), but calculated for the silicon photonic nanostructure in *x*-polarized excitation.

The spectrum of the effective permittivity of the silicon photonic nanostructure, on the other hand, presents a series of complex features, which are the result of several phenomena. Thus, the two main resonances of the effective permittivity are due the excitation of the two optical modes of the PhC cavity. The spectral separation between the frequencies of the two cavity modes is relatively small and this leads to interference features in the spectrum of the effective permittivity. The other, weaker spectral peaks are presumably due to leaky modes of the PhC slab. Note also that whereas the effective permittivity of the graphene metasurface is isotropic, that of the silicon photonic nanostructure is anisotropic.

### B. VALIDATION OF THE HOMOGENIZATION APPROACH

In order to validate the conclusions drawn in the preceding subsection and to investigate the situations in which our homogenization method is accurate, we calculated the absorption, $A$, reflectance, $R$, and transmittance, $T$ of both metasurfaces and their homogenized counterparts. The main results of these calculations are summarized in figure 7 and they reveal several important ideas. Thus, it can be seen in this figure that in the case of the graphene metasurface the resonances of the transmittance occur at the same wavelengths as the resonances of the effective permittivity, whereas for the silicon photonic nanostructure the two sets of resonances differ to some extent. In order to explain these results, one should note that generally the resonances of the transmittance of a planar optical system correspond to excitation of bound modes of the optical system. In the cases investigated here, the bound modes are localized surface plasmons of graphene crosses for the graphene metasurface and optical modes of the PhC cavities and leaky modes of the PhC slab. Moreover,

**FIGURE 7.** a) Wavelength dependence of absorption, reflectance, and transmittance of the graphene metasurface (solid lines) and its homogenized counterpart (marked with circles). b) The same as in a), but determined for the silicon photonic nanostructure. The spectra corresponding to the homogenized metasurface are depicted with dotted lines.



**FIGURE 8.** Spectra of absorption, reflectance, and transmittance, calculated for different values of the angle of incidence: a) $\theta = 0$, b) $\theta = 30°$, and c) $\theta = 60°$.

the excitation of these resonances induces a resonant response of the medium, via the polarization of the medium, which in turn leads to resonances in the spectrum of the effective permittivity of the homogenized metasurfaces.

Figure 7(b) also shows that whereas the linear optical responses of the graphene metasurface and its homogenized counterpart are almost identical, in the case of the silicon photonic nanostructure they markedly differ from each other. The main reason for this dichotomy is that the graphene crosses are much smaller than the operating wavelength, which makes them respond to the incident optical field as if they were point-like resonators. By contrast, the size of the PhC cavities (more precisely, the size of the optical modes) is larger but comparable to the resonance wavelength of the cavity modes, which renders our homogenization method to be only qualitatively valid. It should also be noted, however, that although the homogenization approach for silicon photonic nanostructures does not provide accurate quantitative values for the effective permittivity, it can still provide us valuable qualitative insights into the governing physics.

These ideas are further illustrated by the dependence of the linear optical response of the graphene metasurface on the angle of incidence, $\theta$, of the incoming plane wave, which is presented in figure 8. Thus, it can be observed that the spectral resonances of the graphene metasurface, calculated for $\theta = 0°$, 30° and 60°, only slightly varies with $\theta$, whereas the values of $A$, $R$, and $T$ at the resonance wavelengths depend more pronouncedly on $\theta$. These findings are explained by the fact that the plasmon resonances depend chiefly on the
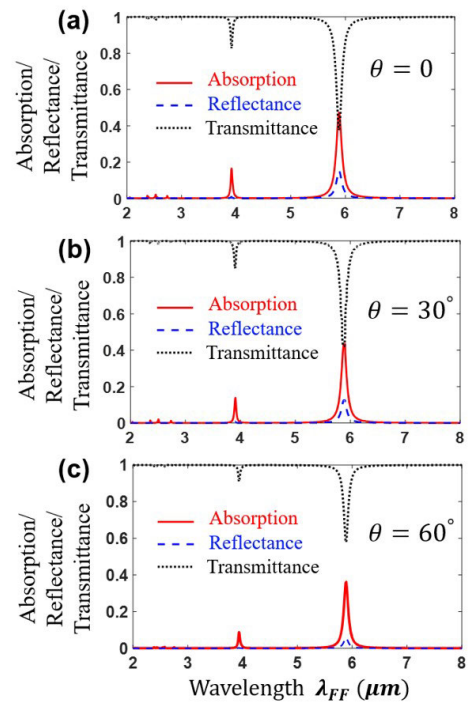
shape of the graphene nano-patches, and thus are independent on $\theta$, whereas the particular values of $A$, $R$, and $T$ depend on the coupling between the incident field and graphene crosses, more specifically on the spatial overlap between the incident wave and the optical field of the graphene plasmons, which is obviously $\theta$-dependent.

### C. EFFECTIVE SECOND-HARMONIC SUSCEPTIBILITY OF GRAPHENE METASURFACES

Let us now consider the nonlinear optical properties of the two optical structures and start with the graphene metasurface. The excitation of graphene localized plasmons at the fundamental frequency (FF) induces a strong optical near-field and consequently enhanced nonlinear polarization, which is the source of the generated SH. The resonance wavelength of these plasmons, and consequently the wavelengths at which enhanced SHG is observed, depends on the graphene permittivity, as per Eq. (1) and Eq. (2), and implicitly on the chemical potential $\mu_c$ and relaxation time $\tau$ of graphene. In particular, as it can be seen in figure 9(a), when the chemical potential increases from 0.2 eV to 0.6 eV, the plasmon wavelength decreases from 11 µm to 6 µm, whereas the corresponding peak absorption increases from 0.25 to 0.48. This dependence of the resonance wavelength on the chemical potential can be explained as follows: when $\mu_c$ increases, the real part of the index of refraction of graphene decreases and consequently the resonance wavelength of the plasmons decreases. Note that in practice it is relatively easy to bias graphene metasurfaces, even when the graphene
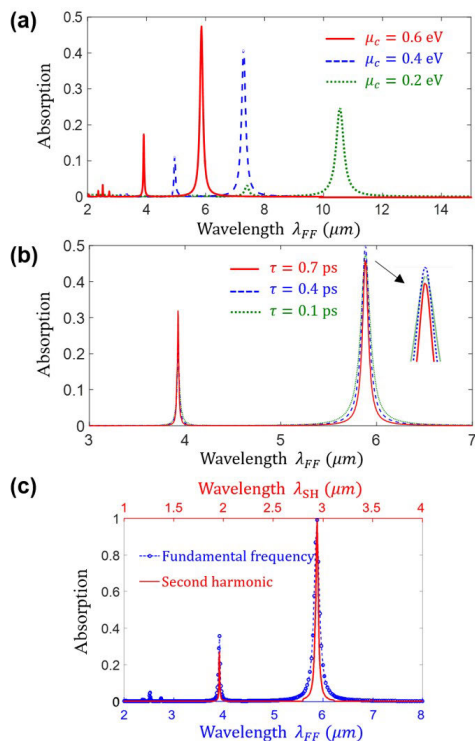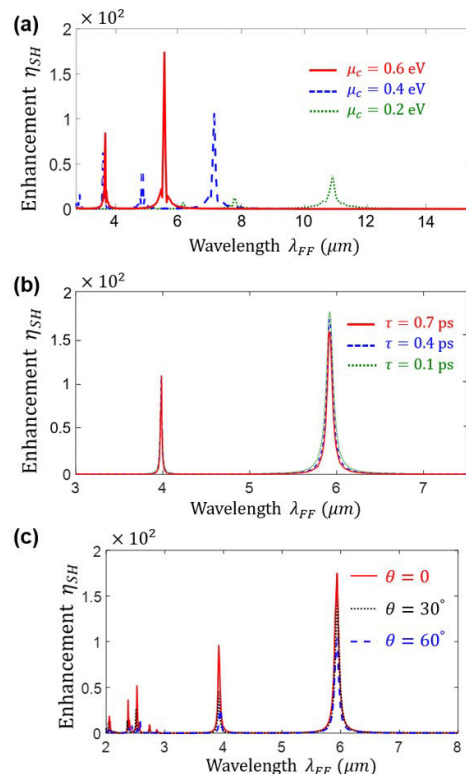
**FIGURE 9.** (a) Spectrum of optical absorption at fundamental frequency calculated for different values of chemical potential, $\mu_c$. (b) Spectrum of optical absorption at fundamental frequency calculated for different values of scattering rate $\tau$. (c) Spectra of the normalized optical absorption at FF (blue curve) and SH (red curve) with rigorous numerical method rather than homogenization.



**FIGURE 10.** (a) Enhancement of effective SH susceptibility of the graphene metasurface, determined for different values of chemical potential, $\mu_c$. (b) Enhancement of effective SH susceptibility of the graphene metasurface, determined for different values of scattering rate, $\tau$. (c) Enhancement of effective SH susceptibility of the graphene metasurface, determined for different values of the angle of incidence, $\theta$.

regions form a noncontiguous area, e.g. by using an ion-gel gating technique [70], [71].

The influence of graphene relaxation time on the absorption of the graphene metasurface is illustrated in figure 9(b). Thus, it can be inferred from this figure that the relaxation time $\tau$ has essentially no effect on the resonance wavelength of the graphene plasmons because the graphene permittivity depends only weakly on $\tau$. Moreover, as expected, the spectral width of the resonance becomes narrower as the relaxation time increases, which is a consequence of the fact that when the relaxation time increases, graphene losses decrease.

The enhancement of the linear and nonlinear optical response of the graphene metasurface can be clearly seen in figure 9(c), where we present the normalized absorption spectra at the FF and SH. In particular, it can be observed in this figure that the occurrence of a resonance at the FF is accompanied by a resonance at half of its wavelength in the SH spectrum. For example, the plasmon resonance at the FF of $\lambda_{FF} = 5.878\,\mu m$ has a correspondent in the SH spectrum at $\lambda_{SH} = \lambda_{FF}/2 = 2.939\,\mu m$.

As can be easily inferred from Eq. (9) and Eq. (10), the dominant components (in absolute value) of the second-order susceptibility of graphene are $\chi_{g,xxyy}^{(2)} = \chi_{g,yyxx}^{(2)}$. The value of this component, determined for a FF wavelength $\lambda = 1\,\mu m$, is $\chi_{g,xxyy}^{(2)} = (-8.37 + 0.133i) \times 10^{-19}\,m^2\,V^{-1}$. Moreover, as a consequence of our approach to the

calculation of the effective second-order susceptibility, it is equal to zero for the same set of indices for which the graphene second-order susceptibility is equal to zero. Therefore, in order to quantify the enhancement of the nonlinear optical response of the graphene metasurface, we computed the enhancement factor, $\eta_{SH} = |\overline{\chi}_{xxyy}^{(2)}/\chi_{g,xxyy}^{(2)}|$, for several values of the chemical potential, $\mu_c = 0.2\,eV$, $0.4\,eV$ and $0.6\,eV$ [see figures 10(a)] and angle of incidence, $\theta = 0°$, $30°$ and $60°$, as per figure 10(c).

The most important conclusion of this analysis is that, at the wavelength of the fundamental plasmon, the effective second-order susceptibility of the homogenized graphene metasurface is enhanced by almost $200\times$. More precisely, the maximum achievable enhancement factor is $\eta_{SH} = 175$, which means that the maximum value of the effective second-order susceptibility of the homogenized graphene metasurface is $|\overline{\chi}_{xxyy}^{(2)}| = 1.46 \times 10^{-16}\,m^2\,V^{-1}$. For comparison, the bulk second-order susceptibility of two centrosymmetric materials widely used in nonlinear optics, gold and silicon, are $\gamma = 7.13 \times 10^{-21}\,m^2\,V^{-1}$ (gold at $\lambda = 810\,nm$) [72] and $\gamma = 1.3 \times 10^{-19}\,m^2\,V^{-1}$ (silicon at $\lambda = 800\,nm$) [73]. Moreover, it can be seen in figure 10(a) that the enhancement factor $\eta_{SH}$ increases with the chemical potential $\mu_c$, namely it increases by almost $4\times$ when $\eta_{SH}$ increases from $0.2\,eV$ to $0.6\,eV$. In addition, it can be inferred from figure 10(c)

that the enhancement factor is smaller for higher-order plasmons, as in this case the plasmon-induced field enhancement decreases. Another feature revealed by figure 10(c) is that the enhancement factor decreases as the angle of incidence increases, a finding explained by the fact that when $\theta$ increases the spatial overlap between the incident wave and the plasmon mode becomes less favorable and thus the enhancement of the local optical field decreases.

### D. EFFECTIVE RAMAN SUSCEPTIBILITY OF THE SILICON PHOTONIC CRYSTAL METASURFACE

Due to the symmetry properties of the silicon photonic nanostructure and the orientation of the cavity array with respect to the principal axes of silicon, the only non-zero component of the effective Raman susceptibility of the photonic nanostructure is $\overline{\chi}_{R,1212}^{(3)} \equiv \overline{\chi}_{R}^{(3)}$. Therefore, similarly to the case of the graphene metasurface, we define the enhancement factor $\eta_R = |\overline{\chi}_R^{(3)}/\chi_R^{(3)}|$, where $\chi_R^{(3)} \equiv \chi_{R,1212}^{(3)}$ is the dominant component of the Raman susceptibility of silicon. The parameter $\eta_R$ quantifies the enhancement of the Raman nonlinearity of the silicon photonic nanostructure. Moreover, in order to investigate the dependence of the enhancement factor on the angle of incidence, these calculations were performed for $\theta = 0°$, $30°$ and $60°$.

Following the procedure we just described, we found out that for the values of the incidence angle of $0°$, $30°$ and $60°$, the enhancement factor was $2.29 \times 10^4$, $3.19 \times 10^3$ and $1.99 \times 10^3$, respectively. Thus, it can be seen that a giant enhancement of the effective Raman susceptibility of the silicon photonic nanostructure of more than 4 orders of magnitude can be achieved at normal incidence. In order to understand the main reason for this remarkable nonlinearity enhancement, one should note that due to the large $Q$-factor of the pump and Stokes cavity modes the field is significantly enhanced as compared to the amplitude of the incident wave, which in conjunction with the fact that the Raman intensity is proportional to the local field to the power of 6, leads to the extremely large resonant enhancement of the Raman response of the silicon photonic nanostructure. Moreover, the cavity field enhancement decreases when the angle of incidence increases, due to a weaker coupling between the incoming wave and the cavity modes, which results in reduced nonlinearity enhancement at larger $\theta$.

As a final remark, it should be noted that the specific design of our metasurface ensures a particularly efficient Raman amplification. To be more specific, let us compare the spectral width of Raman interaction in silicon, $\Delta\nu_R = 105\,\text{GHz}$ [74], with the spectral width of the cavity mode at the Stokes frequency, $\Delta\nu_S = \omega_S/(2\pi Q_S) = 2.1\,\text{GHz}$. Thus, since $\Delta\nu_S \ll \Delta\nu_R$, an efficient Raman interaction can be achieved.

### V. CONCLUSION

In summary, two generic metasurfaces, a graphene metasurface based on graphene cruciform patches and a silicon photonic nanostructure with photonic crystal cavities as building blocks, are studied using a versatile and powerful homogenization method. In particular, in order to quantify the linear and nonlinear optical response of the two metasurfaces, we computed their effective permittivities and nonlinear susceptibilities. Our calculations revealed that, in both cases, the nonlinear optical response of the metasurfaces was enhanced by several orders of magnitude at the resonances of the metasurface building blocks. Moreover, by comparing the optical response of the metasurfaces and their homogenized counterparts, we showed that the homogenization approach is more suitable for graphene-based metasurfaces, because in this case the size of the resonant graphene nanostructures is much smaller than the operating wavelength. Even though the homogenization approach for silicon photonic nanostructures appeared to be less accurate, it could still provide valuable qualitative insights into their nonlinear optical response.

It should be noted that our homogenization approach is rather general, in that it can be readily extended to metasurfaces of different configurations or made of optical media with various dispersive and nonlinear optical properties. Moreover, the ideas presented in this article have broad applicability, as they can be easily extended to other nonlinear optical interactions of practical interest, including third-harmonic generation, four-wave mixing, and sum- and difference frequency generation.

### REFERENCES

[1] M. Veysi, C. Guclu, O. Boyraz, and F. Capolino, "Thin anisotropic metasurfaces for simultaneous light focusing and polarization manipulation," *J. Opt. Soc. Amer. B, Opt. Phys.*, vol. 32, no. 2, pp. 318–323, Jan. 2015.

[2] G. Ren, Z. Lai, C. Wang, Q. Feng, L. Liu, K. Liu, and X. Luo, "Subwavelength focusing of light in the planar anisotropic metamaterials with zone plates," *Opt. Express*, vol. 18, no. 17, pp. 18151–18157, Jul. 2010.

[3] C. Ma and Z. Liu, "Focusing light into deep subwavelength using metamaterial immersion lenses," *Opt. Express*, vol. 18, no. 5, pp. 4838–4844, Feb. 2010.

[4] S. Maslovski and S. Tretyakov, "Perfect lensing with phase-conjugating surfaces: Toward practical realization," *New J. Phys.*, vol. 14, no. 3, Mar. 2012, Art. no. 035007.

[5] G. Rosenblatt and M. Orenstein, "Perfect lensing by a single interface: Defying loss and bandwidth limitations of metamaterials," *Phys. Rev. Lett.*, vol. 115, no. 19, Nov. 2015, Art. no. 195504.

[6] N. I. Landy, S. Sajuyigbe, J. J. Mock, D. R. Smith, and W. J. Padilla, "Perfect metamaterial absorber," *Phys. Rev. Lett.*, vol. 100, no. 20, May 2008, Art. no. 207402.

[7] S. Feng and K. Halterman, "Coherent perfect absorption in epsilon-near-zero metamaterials," *Phys. Rev. B, Condens. Matter*, vol. 86, no. 16, Oct. 2012, Art. no. 165103.

[8] R. Alaee, M. Farhat, C. Rockstuhl, and F. Lederer, "A perfect absorber made of a graphene micro-ribbon metamaterial," *Opt. Express*, vol. 20, no. 27, pp. 28017–28024, Dec. 2012.

[9] Y. Jin, S. Xiao, N. A. Mortensen, and S. He, "Arbitrarily thin metamaterial structure for perfect absorption and giant magnification," *Opt. Express*, vol. 19, no. 12, pp. 11114–11119, Jun. 2011.

[10] S. Song, Q. Chen, L. Jin, and F. Sun, "Great light absorption enhancement in a graphene photodetector integrated with a metamaterial perfect absorber," *Nanoscale*, vol. 5, no. 20, pp. 9615–9619, Aug. 2013.

[11] D. Schurig, J. J. Mock, B. J. Justice, S. A. Cummer, J. B. Pendry, A. F. Starr, and D. R. Smith, "Metamaterial electromagnetic cloak at microwave frequencies," *Science*, vol. 314, no. 5801, pp. 977–980, Nov. 2006.

[12] P. Alitalo and S. Tretyakov, "Electromagnetic cloaking with metamaterials," *Mater. Today*, vol. 12, no. 3, pp. 22–29, Mar. 2009.

[13] D. Shin, Y. Urzhumov, Y. Jung, G. Kang, S. Baek, M. Choi, H. Park, K. Kim, and D. R. Smith, "Broadband electromagnetic cloaking with smart metamaterials," *Nature Commun.*, vol. 3, no. 1, pp. 1–8, Nov. 2012.

[14] C. Luo, S. G. Johnson, J. D. Joannopoulos, and J. B. Pendry, "Subwavelength imaging in photonic crystals," *Phys. Rev. B, Condens. Matter*, vol. 68, no. 4, Jul. 2003, Art. no. 045115.

[15] S. Foteinopoulou and C. M. Soukoulis, "Electromagnetic wave propagation in two-dimensional photonic crystals: A study of anomalous refractive effects," *Phys. Rev. B, Condens. Matter*, vol. 72, no. 16, 2005, Art. no. 165112.

[16] T. Decoopman, G. Tayeb, S. Enoch, D. Maystre, and B. Gralak, "Photonic crystal lens: From negative refraction and negative index to negative permittivity and permeability," *Phys. Rev. Lett.*, vol. 97, no. 7, Aug. 2006, Art. no. 073905.

[17] Z. Liu, S. Durant, H. Lee, Y. Pikus, Y. Xiong, C. Sun, and X. Zhang, "Experimental studies of far-field superlens for sub-diffractional optical imaging," *Opt. Express*, vol. 15, no. 11, pp. 6947–6954, 2007.

[18] R. Chatterjee, N. C. Panoiu, K. Liu, Z. Dios, M. B. Yu, M. T. Doan, L. J. Kaufman, R. M. Osgood, and C. W. Wong, "Achieving subdiffraction imaging through bound surface states in negative refraction photonic crystals in the near-infrared range," *Phys. Rev. Lett.*, vol. 100, no. 18, May 2008, Art. no. 187401.

[19] E. J. Osley, C. G. Biris, P. G. Thompson, R. R. F. Jahromi, P. A. Warburton, and N. C. Panoiu, "Fano resonance resulting from a tunable interaction between molecular vibrational modes and a double continuum of a plasmonic metamolecule," *Phys. Rev. Lett.*, vol. 110, no. 8, Feb. 2013, Art. no. 087402.

[20] A. V. Kabashin, P. Evans, S. Pastkovsky, W. Hendren, G. A. Wurtz, R. Atkinson, R. Pollard, V. A. Podolskiy, and A. V. Zayats, "Plasmonic nanorod metamaterials for biosensing," *Nature Mater.*, vol. 8, no. 11, pp. 867–871, Nov. 2009.

[21] K. V. Sreekanth, Y. Alapan, M. ElKabbash, E. Ilker, M. Hinczewski, U. A. Gurkan, A. De Luca, and G. Strangi, "Extreme sensitivity biosensing platform based on hyperbolic metamaterials," *Nature Mater.*, vol. 15, no. 6, pp. 621–627, Jun. 2016.

[22] C. Cao, J. Zhang, X. Wen, S. L. Dodson, N. T. Dao, L. M. Wong, S. Wang, S. Li, A. T. Phan, and Q. Xiong, "Metamaterials-based label-free nanosensor for conformation and affinity biosensing," *ACS Nano*, vol. 7, no. 9, pp. 7583–7591, Sep. 2013.

[23] I. Al-Naib, G. Sharma, M. M. Dignam, H. Hafez, A. Ibrahim, D. G. Cooke, T. Ozaki, and R. Morandotti, "Effect of local field enhancement on the nonlinear terahertz response of a silicon-based metamaterial," *Phys. Rev. B, Condens. Matter*, vol. 88, no. 19, 2013, Art. no. 195203.

[24] P. Ding, E. Liang, G. Cai, W. Hu, C. Fan, and Q. Xue, "Dual-band perfect absorption and field enhancement by interaction between localized and propagating surface plasmons in optical metamaterials," *J. Opt.*, vol. 13, no. 7, 2011, Art. no. 075005.

[25] J. Zhang, W. Liu, Z. Zhu, X. Yuan, and S. Qin, "Strong field enhancement and light-matter interactions with all-dielectric metamaterials based on split bar resonators," *Opt. Express*, vol. 22, no. 25, pp. 30889–30898, 2014.

[26] Z. Liu, A. Boltasseva, R. H. Pedersen, R. Bakker, A. V. Kildishev, V. P. Drachev, and V. M. Shalaev, "Plasmonic nanoantenna arrays for the visible," *Metamaterials*, vol. 2, no. 1, pp. 45–51, 2008.

[27] B. Kante, A. de Lustrac, and J. M. Lourtioz, "In-plane coupling and field enhancement in infrared metamaterial surfaces," *Phys. Rev. B, Condens. Matter*, vol. 80, no. 3, 2009, Art. no. 035108.

[28] M. R. Shcherbakov, D. N. Neshev, B. Hopkins, A. S. Shorokhov, I. Staude, E. V. Melik-Gaykazyan, M. Decker, A. A. Ezhov, A. E. Miroshnichenko, I. Brener, A. A. Fedyanin, and Y. S. Kivshar, "Enhanced third-harmonic generation in silicon nanoparticles driven by magnetic response," *Nano Lett.*, vol. 14, no. 11, pp. 6488–6492, 2014.

[29] W. Fan, S. Zhang, N.-C. Panoiu, A. Abdenour, S. Krishna, R. M. Osgood, K. J. Malloy, and S. R. J. Brueck, "Second harmonic generation from a nanopatterned isotropic nonlinear material," *Nano Lett.*, vol. 6, no. 5, pp. 1027–1030, 2006.

[30] S. Kruk, M. Weismann, A. Y. Bykov, E. A. Mamonov, I. A. Kolmychek, T. Murzina, N. C. Panoiu, D. N. Neshev, and Y. S. Kivshar, "Enhanced magnetic second-harmonic generation from resonant metasurfaces," *ACS Photon.*, vol. 2, no. 8, pp. 1007–1012, 2015.

[31] N. C. Panoiu and R. M. Osgood, "Enhanced optical absorption for photovoltaics via excitation of waveguide and plasmon-polariton modes," *Opt. Lett.*, vol. 32, no. 19, pp. 2825–2827, 2007.

[32] J. S. Gomez-Diaz, M. Tymchenko, J. Lee, M. A. Belkin, and A. Alu, "Nonlinear processes in multi-quantum-well plasmonic metasurfaces: Electromagnetic response, saturation effects, limits, and potentials," *Phys. Rev. B, Condens. Matter*, vol. 92, no. 12, 2015, Art. no. 125429.

[33] A. Rose and D. R. Smith, "Overcoming phase mismatch in nonlinear metamaterials," *Opt. Mater. Express*, vol. 1, no. 7, pp. 1232–1243, 2011.

[34] C. Argyropoulos, G. D. Aguanno, and A. Alu, "Giant second-harmonic generation efficiency and ideal phase matching with a double e-near-zero cross-slit metamaterial," *Phys. Rev. B, Condens. Matter*, vol. 89, no. 23, 2014, Art. no. 235401.

[35] E. Almeida, G. Shalem, and Y. Prior, "Subwavelength nonlinear phase control and anomalous phase matching in plasmonic metasurfaces," *Nature Commun.*, vol. 7, no. 1, pp. 1–7, 2016.

[36] G. Li, S. Zhang, and T. Zentgraf, "Nonlinear photonic metasurfaces," *Nat. Rev. Mater.*, vol. 2, no. 5, 2017, Art. no. 17010.

[37] F. Qin, L. Ding, L. Zhang, F. Monticone, C. C. Chum, J. Deng, S. Mei, Y. Li, J. Teng, M. Hong, S. Zhang, A. Alu, and C. W. Qiu, "Hybrid bilayer plasmonic metasurface efficiently manipulates visible light," *Sci. Adv.*, vol. 2, no. 1, 2016, Art. no. e1501168.

[38] Y. Zhao and A. Alù, "Manipulating light polarization with ultrathin plasmonic metasurfaces," *Phys. Rev. B, Condens. Matter*, vol. 84, no. 20, 2011, Art. no. 205428.

[39] Y. Yang, I. I. Kravchenko, D. P. Briggs, and J. Valentine, "All-dielectric metasurface analogue of electromagnetically induced transparency," *Nature Commun.*, vol. 5, no. 1, pp. 1–7, 2014.

[40] J. Sautter, I. Staude, M. Decker, E. Rusak, D. N. Neshev, I. Brener, and Y. S. Kivshar, "Active tuning of all-dielectric metasurfaces," *ACS Nano*, vol. 9, no. 4, pp. 4308–4315, Apr. 2015.

[41] J. B. Khurgin, "How to deal with the loss in plasmonics and metamaterials," *Nature Nanotechnol.*, vol. 10, no. 1, pp. 2–6, Jan. 2015.

[42] G. V. Naik, J. Kim, and A. Boltasseva, "Oxides and nitrides as alternative plasmonic materials in the optical range," *Opt. Mater. Express*, vol. 1, no. 6, pp. 1090–1099, 2011.

[43] K. Tanaka, E. Plum, J. Y. Ou, T. Uchino, and N. I. Zheludev, "Multifold enhancement of quantum dot luminescence in plasmonic metamaterials," *Phys. Rev. Lett.*, vol. 105, no. 22, Nov. 2010, Art. no. 227403.

[44] D. R. Smith, S. Schultz, P. Markoš, and C. M. Soukoulis, "Determination of effective permittivity and permeability of metamaterials from reflection and transmission coefficients," *Phys. Rev. B, Condens. Matter*, vol. 65, no. 19, Apr. 2002, Art. no. 195104.

[45] D. R. Smith and J. B. Pendry, "Homogenization of metamaterials by field averaging," *J. Opt. Soc. Amer. B, Opt. Phys.*, vol. 23, no. 3, pp. 391–403, 2006.

[46] S. Larouche and D. R. Smith, "A retrieval method for nonlinear metamaterials," *Opt. Commun.*, vol. 283, no. 8, pp. 1621–1627, 2010.

[47] M. A. Gorlach, T. A. Voytova, M. Lapine, Y. S. Kivshar, and P. A. Belov, "Nonlocal homogenization for nonlinear metamaterials," *Phys. Rev. B, Condens. Matter*, vol. 93, Apr. 2016, Art. no. 165125.

[48] B. Wells, A. Y. Bykov, G. Marino, M. E. Nasir, A. V. Zayats, and V. A. Podolskiy, "Structural second-order nonlinearity in plasmonic metamaterials," *Optica*, vol. 5, no. 12, pp. 1502–1507, 2018.

[49] S. V. Li, Y. S. Kivshar, and M. V. Rybin, "Toward silicon-based metamaterials," *ACS Photon.*, vol. 5, no. 12, pp. 4751–4757, Dec. 2018.

[50] J. W. You and N. C. Panoiu, "Plasmon-induced nonlinearity enhancement and homogenization of graphene metasurfaces," *Opt. Lett.*, vol. 44, no. 12, pp. 3030–3033, 2019.

[51] F. H. L. Koppens, D. E. Chang, and F. J. G. de Abajo, "Graphene plasmonics: A platform for strong light–matter interactions," *Nano Lett.*, vol. 11, no. 8, pp. 3370–3377, Jul. 2011.

[52] S. H. Lee, M. Choi, T.-T. Kim, S. Lee, M. Liu, X. Yin, H. K. Choi, S. S. Lee, C.-G. Choi, S.-Y. Choi, X. Zhang, and B. Min, "Switching terahertz waves with gate-controlled active graphene metamaterials," *Nature Mater.*, vol. 11, no. 11, pp. 936–941, 2012.

[53] Z. Li, K. Yao, F. Xia, S. Shen, J. Tian, and Y. Liu, "Graphene plasmonic metasurfaces to steer infrared light," *Sci. Rep.*, vol. 5, no. 1, Dec. 2015, Art. no. 12423.

[54] X. Chen, W. Fan, and C. Song, "Multiple plasmonic resonance excitations on graphene metamaterials for ultrasensitive terahertz sensing," *Carbon*, vol. 133, pp. 416–422, Jul. 2018.

[55] T. F. Heinz, "Second-order nonlinear optical effects at surfaces and interfaces," in *Nonlinear Surface Electromagnetic Phenomena* (Modern Problems in Condensed Matter Sciences), vol. 29, H. E. Ponath and G. I. Stegeman, Eds. Amsterdam, The Netherlands: Elsevier, 1991, pp. 353–416.

[56] N. C. Panoiu, W. E. I. Sha, D. Y. Lei, and G. C. Li, "Nonlinear optics in plasmonic nanostructures," *J. Opt.*, vol. 20, no. 8, 2018, Art. no. 083001.

[57] Q. Ren, J. W. You, and N. C. Panoiu, "Giant enhancement of the effective Raman susceptibility in metasurfaces made of silicon photonic crystal nanocavities," *Opt. Express*, vol. 26, no. 23, pp. 30383–30392, 2018.

[58] J. W. You, S. R. Bongu, Q. Bao, and N. C. Panoiu, "Nonlinear optical properties and applications of 2D materials: Theoretical and experimental aspects," *Nanophotonics*, vol. 8, no. 1, pp. 63–97, Dec. 2018.

[59] P. A. D. Goncalves and N. M. Peres, *An Introduction to Graphene Plasmonics*. Singapore: World Scientific, 2016.

[60] X. Yang and C. W. Wong, "Design of photonic band gap nanocavities for stimulated Raman amplification and lasing in monolithic silicon," *Opt. Express*, vol. 13, no. 12, pp. 4723–4730, 2005.

[61] P. A. Temple and C. E. Hathaway, "Multiphonon Raman spectrum of silicon," *Phys. Rev. B, Condens. Matter*, vol. 7, no. 8, 1973, Art. no. 3685.

[62] P. G. Thompson, C. G. Biris, E. J. Osley, O. Gaathon, R. M. Osgood, N. C. Panoiu, and P. A. Warburton, "Polarization-induced tunability of localized surface plasmon resonances in arrays of sub-wavelength cruciform apertures," *Opt. Express*, vol. 19, no. 25, pp. 25035–25047, 2011.

[63] Q. Ren, J. W. You, and N. C. Panoiu, "Large enhancement of the effective second-order nonlinearity in graphene metasurfaces," *Phys. Rev. B, Condens. Matter*, vol. 99, no. 20, May 2019, Art. no. 205404.

[64] J. D. Cox, I. Silveiro, and F. J. G. de Abajo, "Quantum effects in the nonlinear response of graphene plasmons," *ACS Nano*, vol. 10, no. 2, pp. 1995–2003, 2016.

[65] B. Jalali and S. Fathpour, "Silicon photonics," *J. Lightw. Technol.*, vol. 24, no. 12, pp. 4600–4615, Dec. 2006.

[66] *CST Studio Suit*. [Online]. Available: https://www.cst.com

[67] J. W. You, E. Threlfall, D. F. G. Gallagher, and N. C. Panoiu, "Computational analysis of dispersive and nonlinear 2D materials by using a GS-FDTD method," *J. Opt. Soc. Amer. B, Opt. Phys.*, vol. 35, no. 11, pp. 2754–2763, 2018.

[68] *BandSOLVE*. [Online]. Available: https://www.synopsys.com

[69] A. F. Oskooi, D. Roundy, M. Ibanescu, P. Bermel, J. D. Joannopoulos, and S. G. Johnson, "Meep: A flexible free-software package for electromagnetic simulations by the FDTD method," *Comput. Phys. Commun.*, vol. 181, no. 3, pp. 687–702, Mar. 2010.

[70] Z. Miao, Q. Wu, X. Li, Q. He, K. Ding, Z. An, Y. Zhang, and L. Zhou, "Widely tunable terahertz phase modulation with gate-controlled graphene metasurfaces," *Phys. Rev. X*, vol. 5, no. 4, Nov. 2015, Art. no. 041027.

[71] L. Ju, B. Geng, J. Horng, C. Girit, M. Martin, Z. Hao, H. A. Bechtel, X. Liang, A. Zettl, Y. R. Shen, and F. Wang, "Graphene plasmonics for tunable terahertz metamaterials," *Nature Nanotechnol.*, vol. 6, no. 10, pp. 630–634, Sep. 2011.

[72] D. Krause, C. W. Teplin, and C. T. Rogers, "Optical surface second harmonic measurements of isotropic thin-film metals: Gold, silver, copper, aluminum, and tantalum," *J. Appl. Phys.*, vol. 96, no. 7, pp. 3626–3634, Oct. 2004.

[73] M. Falasconi, L. C. Andreani, A. M. Malvezzi, M. Patrini, V. Mulloni, and L. Pavesi, "Bulk and surface contributions to second-order susceptibility in crystalline and porous silicon by second-harmonic generation," *Surf. Sci.*, vol. 481, nos. 1–3, pp. 105–112, Jun. 2001.

[74] R. M. Osgood, N. C. Panoiu, J. I. Dadap, X. Liu, X. Chen, I. W. Hsieh, E. Dulkeith, W. M. J. Green, and Y. A. Vlasov, "Engineering nonlinearities in nanoscale optical systems: Physics and applications in dispersion-engineered silicon nanophotonic wires," *Adv. Opt. Photon.*, vol. 1, no. 1, pp. 162–235, Jan. 2009.

**QUN REN** received the B.Sc. degree from the School of Electronic Information Engineering, Tianjin University, Tianjin, China, in 2015, and the Ph.D. degree from University College London, U.K., in 2019.

From January 2014 to May 2014, she was a Visiting Scholar with the School of Electrical and Electronic Engineering, Nanyang Technological University, Singapore. Her research interests include metasurfaces, computational electromagnetics, terahertz generation, nonlinear plasmonics, and quantum optics.

**JIAN WEI YOU** (Member, IEEE) received the B.Sc. degree in electrical engineering from Xidian University, Xi'an, China, in 2010, and the Ph.D. degree in electromagnetic and microwave technology from Southeast University, Nanjing, China, in 2016. From July 2011 to December 2011, he was as a Research Visitor with the Department of Electrical and Computer Engineering, University of Houston, Houston, USA. In January 2016, he joined the Department of Electronic and Electrical Engineering, University College London, as a Research Associate. His research interests include computational electromagnetics, nonlinear microwave and optics, quantum metamaterials, multiphysics, and computational plasma physics.
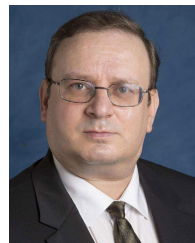
**NICOLAE-CORIOLAN PANOIU** (Member, IEEE) received the B.Sc. and M.S. degrees in physics from the University of Bucharest, Bucharest, Romania, in 1990 and 1992, respectively, and the Ph.D. degree from New York University (NYU), New York City, in 2001. After graduating from NYU, he was a Postdoctoral Fellow with the Department of Applied Physics and Applied Mathematics, Columbia University, New York City. He is currently a Professor of Nanophotonics with the Department of Electronic and Electrical Engineering, University College London. His research interests include silicon photonics, optical properties of photonic nanostructures and metamaterials, and computational modeling of electromagnetic structures. He is a member of OSA.

● ● ●